Journal of Controlled Release 336 (2021) 40–53

Contents lists available at ScienceDirect

Journal of Controlled Release

journal homepage: www.elsevier.com/locate/jconrel

Simultaneous blockage of contextual TGF-β by cyto-pharmaceuticals to suppress breast cancer metastasis

Yanyi Li [1], Qifan Hu [1], Weishuo Li, Shijing Liu, Kaiming Li, Xiaoyu Li, Junjie Du, Zexuan Yu, Cong Wang [*], Can Zhang [*]

State Key Laboratory of Natural Medicines and Jiangsu Key Laboratory of Drug Discovery for Metabolic Diseases, Center of Advanced Pharmaceuticals and Biomaterials, China Pharmaceutical University, Nanjing 210009, China

ARTICLE INFO

Keywords:
Cyto-pharmaceuticals
Simultaneous blockage
Targeting metastasis
Transforming growth factor-β
Neutrophils

ABSTRACT

It remains challenging to treat tumor metastasis currently in the light of multiple cascade processes of tumor metastasis. Additionally, multiple clinical drugs for metastasis have quite limited therapeutic potential and even facilitate metastasis in preclinical models. Thus, potential metastasis targets and novel metastasis-directed drugs are urgently needed to be further developed. Herein, transforming growth factor-β (TGF-β) is verified to contribute to lung metastasis in a context-dependent manner in the 4T1 orthotopic tumor-bearing mice model, which induces epithelial-mesenchymal-transition (EMT) to promote tumor dissemination from the primary site and dampens the anti-tumor response of neutrophils to support tumor colonization at the metastatic niche. In view of neutrophils' superior tropism towards both inflammatory primary tumor and metastatic niche, SB525334, a TGF-β receptor inhibitor, is loaded into cationic liposome (SBLP) which is subsequently incorporated into neutrophils to yield the cyto-pharmaceuticals (SBLP/NE). The systemically infused SBLP/NE can simultaneously migrate into both primary and metastatic sites, then release SB525334 in response to tumor stimuli, and contextually inhibit TGF-β-mediated-EMT and phenotype reversal of infiltrated neutrophils, showing substantial metastasis suppression efficacy without causing any detectable toxicities. This project shifts the paradigm for metastasis suppression therapy by simultaneous blockage of contextual TGF-β using metastatic-cascades-targeting neutrophil cyto-pharmaceuticals.

1. Introduction

Metastasis is responsible for approximately 90% of tumor-related mortality [1,2], the process of which includes dissemination of tumor cells from the primary site and colonization at the distant organs [3]. Due to an inadequate understanding of the complex biological mechanism, metastatic disease has not been cured efficiently yet.

Currently, there are two kinds of drugs applied in treating metastasis. One is the traditional drug that has been approved by the US Food and Drug Administration (FDA) like paclitaxel, mutant BRAF inhibitors, and cisplatin. These drugs can target tumor growth but are not effective in preventing metastasis, some of which even stimulate metastasis in preclinical models [4]. The other one is a metastasis-directed drug that targets steps in metastatic cascades, such as anti-RANK antibody Denosumab, anti-VEGF antibody Bevacizumab, and integrin peptide inhibitor Cilengitide [4]. However, it is worth noting that most of the current metastasis-directed drugs interrupt either the dissemination or the colonization step, of which metastasis suppression efficiency might be unsatisfactory since multiple stages in the metastatic cascade might have taken place simultaneously in a patient [1,5,6]. With this in mind, we believe simultaneous interruption of the dissemination and colonization are more likely to realize an augmented metastasis suppression efficacy.

Transforming growth factor-β (TGF-β), a secreted cytokine, is highly expressed in the tumor microenvironment [7,8]. Theoretically, TGF-β involves in several tumor metastasis cascades, such as promoting epithelial-mesenchymal-transition (EMT), regulating the immune system, remodeling the matrix, and stimulating angiogenesis [7–10]. However, the metastasis-promoting puzzle of TGF-β at metastatic niche remains largely unexplored with only several studies focusing on bone metastasis [11]. Besides, current TGF-β targeting therapies have demonstrated certain metastasis suppression efficacy [12–14], but

* Corresponding authors.
E-mail addresses: wangcong@cpu.edu.cn (C. Wang), zhangcan@cpu.edu.cn (C. Zhang).
[1] These authors contributed equally to this work.

https://doi.org/10.1016/j.jconrel.2021.06.012
Received 18 March 2021; Received in revised form 18 May 2021; Accepted 9 June 2021
Available online 10 June 2021

further clinical translation and approval of TGF-β inhibitors are challenging due to the unsolved dosage-dependent toxicities towards intestine and heart [14–17]. There is thus a crucial need to develop novel therapeutic strategies to simultaneously deliver TGF-β inhibitors to both primary and metastatic sites, thereby specifically achieving the metastatic-cascades-targeting efficacy of TGF-β.

Recently, the utilization of living cells for drug delivery has drawn much attention. Such strategies using living cells is promising as it not only shrinks the potential immunogenicity of exogenous nanoformulations, but also retains the inherent physiological functions [18,19]. Neutrophils, as one of the most critical and abundant immune cells in the innate immune system, have various natural advantages in drug delivery. Neutrophils are well-known for their phagocytic function, which is ably made use of to effectively load drugs. In addition, recent studies have reported that various factors like chemokines and myeloid-related proteins from the tumor sites can recruit neutrophils [20,21] and neutrophils are found to infiltrate into primary tumor and metastatic niche in mouse models and clinical patients [22]. Therefore, we believe that neutrophils can be utilized as an ideal vehicle for delivering TGF-β inhibitors, based on their chemotaxis towards both primary tumors and metastatic niche.

Herein, we first verified the role of contextual TGF-β in the dissemination and colonization steps of tumor metastasis. To achieve a synergistic therapeutic benefit, we incorporated TGF-β receptor inhibitor (SB525334) loaded liposomes into neutrophils to yield neutrophil cyto-pharmaceuticals based on our previous studies [23–25]. Owing to the superior tropism towards the inflammatory primary tumor [26] and metastatic niche, neutrophil cyto-pharmaceuticals could migrate into both primary tumor and metastatic niche simultaneously (Fig. 1). The accumulated neutrophil cyto-pharmaceuticals unloaded SB525334 characteristically in response to tumor stimuli. At the primary site, the released SB525334 suppressed the EMT process and impeded the dissemination of tumor cells. At the metastatic niche, the released SB525334 unleashed the anti-tumor responses of infiltrated neutrophils and inhibited the colonization. Through simultaneous interruption of both dissemination and colonization steps in metastasis cascades, neutrophil cyto-pharmaceuticals of SB525334 showed a substantial metastasis suppression efficacy without causing any detectable toxicities and provided a new metastasis-inhibiting strategy based on simultaneous inhibition of multiple metastatic cascades.

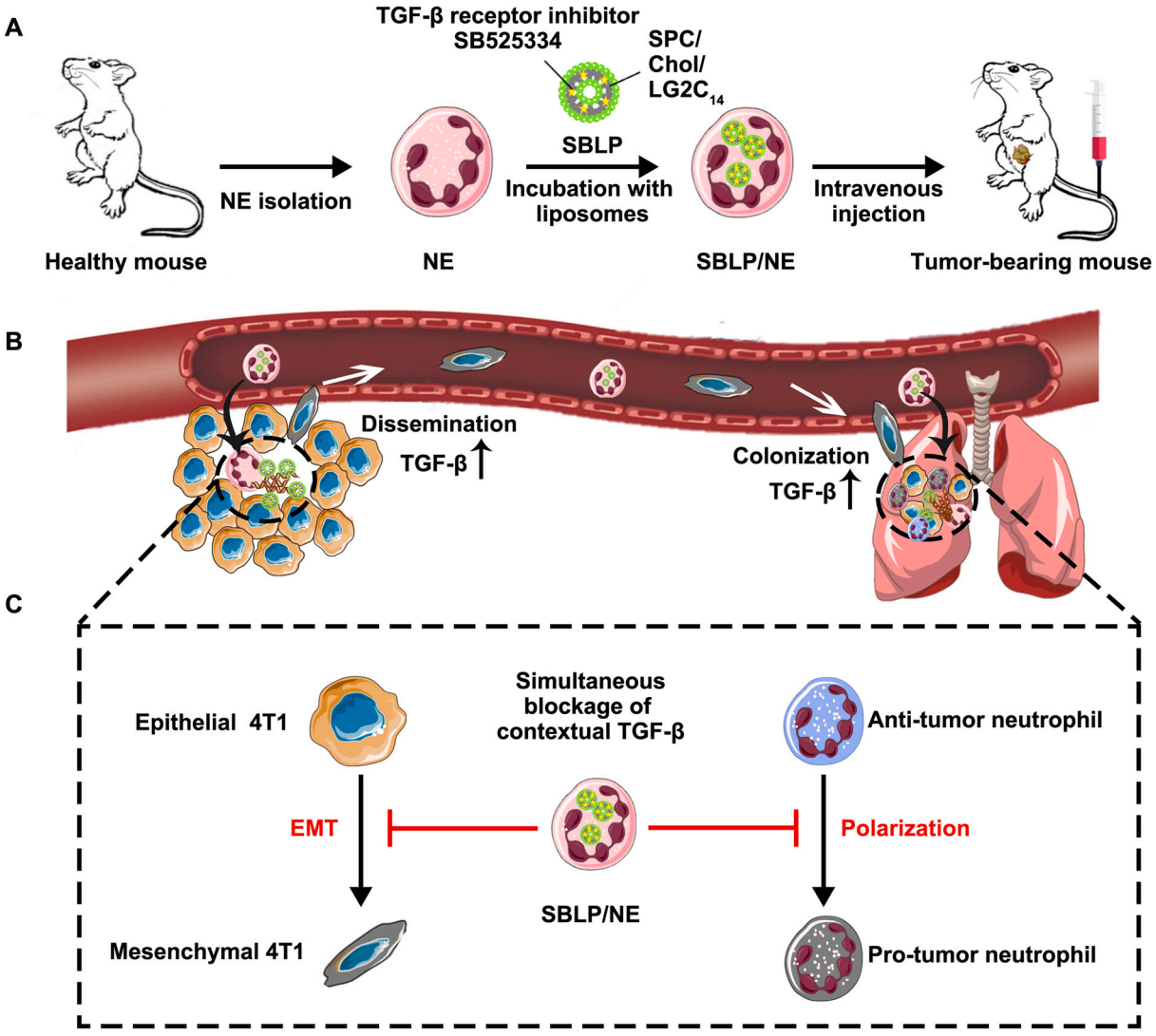

Fig. 1. Schematic illustration of simultaneous blockage of TGF-β by neutrophil cyto-pharmaceuticals to suppress breast tumor lung metastasis. (A) Fabrication of neutrophil cyto-pharmaceuticals of SB525334 (SBLP/NE) by incubation of liposomal SB525334 (SBLP) with allogeneic neutrophils. (B) The accumulation of SBLP/NE into primary tumor and metastatic niche. (C) Simultaneous blockage of TGF-β induced EMT at the primary site and neutrophils' phenotype reversal at metastatic niche by released SB525334.

2. Experimental section

2.1. Cell culture

The mouse breast 4T1 tumor cell line were purchased from the National Collection of Authenticated Cell Cultures. The 4T1 cells were cultured in RPMI 1640 medium containing 10% fetal bovine serum (FBS), 100 U mL^{-1} penicillin, and 0.1 mg mL^{-1} streptomycin. The cells were kept at 37 °C in a humidified atmosphere containing 5% CO_2.

2.2. Establishment of 4 T1 spontaneous lung metastasis animal model

All animals were treated following the Guide for Care and Use of Laboratory Animals, approved by the Animal Experimentation Ethics Committee of China Pharmaceutical University (Nanjing, China, Permit number 2021–05–002). For orthotopic metastasis, 1×10^6 4T1 cells or 4T1-Luc cells suspended in 100 μL PBS were injected into the right mammary fat pad of female BALB/c mice (6–8 weeks, purchased from the Comparative Medicine Center of Yangzhou University), and the lung metastasis was monitored by the IVIS Spectrum *In Vivo* Imaging System (Perkin Elmer, USA).

2.3. Monitoring TGF-β level in metastatic niche

Mice bearing orthotopic 4T1 tumors were sacrificed on day14, 21, and 28. The harvested lungs were homogenized, purified, and acidified for enzyme-linked immunosorbent assays (ELISA) according to the manufacturer's protocol (E-EL-M0051c, Elabscience) to detect the TGF-β1 levels in the lung.

2.4. Evaluation of TGF-β induced EMT at primary site

Briefly, the tumor harvested from mice bearing orthotopic 4T1 tumor on day 28 was embedded with paraffin and cut into slices of 20 mm, which was then subjected to immunohistochemical analysis to verify the expressions of Vimentin (EPR3776, Abcam, 1:200 dilution) and E-cadherin (#3195, Cell Signaling Technology, 1:200 dilution) following the manufacturer's instructions. The relative expression was quantified by the integrated optical density (IOD) using ImageJ pro plus. The relative protein expression = The IOD of SB525334 group / The IOD of the saline group.

For *in vitro* cell experiments, 4T1 cells were treated with TGF-β (10 ng mL^{-1}, AF-100-21C, Pepro Tech) or SB525334 (5 μM, HY-12043, MedChemExpress) unless otherwise stated. For the scratch assay, 4T1 cells were cultured to a density of ~80% in a 24-well plate. A wound was then caused using a 10 μL plastic pipette tip. The wound area at different post-scratch time was monitored and pictured by the microscope (Ts2R, Nikon). Three random fields of wound per well were measured. Wound closure % = (1 – [The average closure distance at different post-scratch time / The average closure distance at post-scratch 0 h]) %.

The expression of EMT-associated proteins, such as Vimentin and E-cadherin, in 4T1 cells treated with TGF-β were quantified. 1×10^6 4 T1 cells were cultured in a 6-well plate for 4 h and then treated with TGF-β or TGF-β plus SB525334 for 36 h, followed by treatment with RIPA Lysis Buffer (P0013B, Beyotime) containing 1% proteinase inhibitor cocktail. All collected samples were normalized using an Enhanced BCA Protein Assay Kit (P0010S, Beyotime) and subsequently subjected to 10% SDS-polyacrylamide gel electrophoresis. Then the separated samples were electrophoretically transferred to polyvinylidene fluoride (PVDF) membranes (0.2 μm, Millipore). The obtained membrane was blocked with 5% non-fat dry milk in tris buffered saline (TBS) at 37 °C for 1 h and incubated with anti-Vimentin (EPR3776, Abcam, 1:1000 dilution), E-cadherin (#3195, Cell Signaling technology, 1:1000 dilution) or β-actin (abs132001, absin, 1:1000 dilution) at 4 °C overnight. Afterwards, the samples were stained by a Goat anti-Rabbit IgG-HRP conjugate (BS13278, Bioworld Technology, 1:10000 dilution) at 37 °C for 1 h, which was incubated with High-sig ECL Western Blotting Substrate (180–5001, Tanon) and immediately pictured by the Automatic Chemiluminescence Imaging System (5200 Multi, Tanon). The expression of Smad2/3 and pSmad2/3 in 4T1 cells and neutrophils was detected by the same method as above, except the primary antibodies, that is Anti-phospho-Smad2/3 antibody (ab254407, Abcam, 1:1000 dilution) and Anti-Smad2/3 antibody (ab202445, Abcam, 1:1000 dilution).

For the qPCR analysis, 5×10^5 4T1 cells were cultured in a 12-well plate for 4 h and then treated with TGF-β or TGF-β plus SB525334 for 36 h, followed by RNA extraction using RNA isolater Total RNA Extraction Reagent (R401–01, Vazyme) according to the manufacturer's instructions. The obtained RNA extracts were used to produce cDNA by HiScript II Q RT SuperMix for qPCR analysis (R223–01, Vazyme). qPCR was performed on a StepOnePlus™ Real-Time PCR System (Applied Biosystems) using qPCR SYBR Green Master Mix (11203ES08, Yeasen). The comparative threshold cycle method was used to calculate gene expression and β-actin was used as a gene reference. Primers used were listed from 5′ to 3′ as followings: *Twist1/2* forward: GGACAAGCTGAGCAAGATTCA, and reverse: CGGAGAAGGCGTAGCTGAG; *Snai1* forward: CCTCAGCAGGGTGGTTACTG, and reverse: CCACTTGGCCCCTAACAAGT; *Actb* forward: GAGAAGATCTGGCACCACACC, and reverse: GCATACAGGGACAGCACAGC.

2.5. Detection of the anti-tumor responses of infiltrated neutrophils in metastatic niche

The lungs harvested from 4T1-bearing mice on day 14, 21 and 28 were manually smashed, digested with 2 mg mL^{-1} collagenase type I (C0130, Sigma) and 1 mg mL^{-1} DNase I (10104159001, Roche) at 37 °C for 30 min, and filtered through a 70 μm nylon cell strainer (352350, Falcon). The obtained single-cell suspension was subjected to centrifugation over a 3-layer discontinuous Percoll (17–0891-09, GE Healthcare) gradient to yield neutrophils. Percoll gradients were prepared by layering 2 mL each of the 62%, and 55% Percoll solutions successively on top of 2 mL of 75% Percoll solution in a conical 15-mL polypropylene tube. The obtained cell suspension was carefully layered on the top of 55% Percoll layer followed by centrifugation (3000 rpm, 30 min), and the cell band located between 75% and 62% Percoll layer was collected and washed triple by phosphate buffer saline (PBS). The isolated neutrophils were stained by fluorescein isothiocyanate (FITC)-conjugated Ly6G antibody (127606, 250 ng mL^{-1}, BioLegend) and Alexa Fluor 647-conjugated $CD11b^+$ antibody (301319, 20 ng mL^{-1}, BioLegend), and analyzed by flow cytometry (Invitrogen, Thermo Fisher Scientific) to determine the purity, activation status as well as the number. The SB-treated neutrophils were isolated from lungs harvested from 4T1-bearing mice on day 28 which receive *i.v.* injection of SB525334 at dosage of 1 mg kg^{-1} every other day from day 7.

The lung harvested on day 21 was embedded by Optimal Cutting Temperature (O.C.T, 4583, Tissue-Tek, SAKURA) and cryosectioned into pieces of 10 mm, which were incubated with FITC-conjugated Ly6G antibody and mounting medium containing DAPI (ZLI-9557, Origene) and subsequently observed by confocal laser scanning microscopy (CLSM, LSM 880, ZEISS). The obtained neutrophils were also stained by Wright-Giemsa (G1007, Servicebio), and observed by an optical microscope (Ts2R, Nikon). The qPCR was performed to verify the phenotype of infiltrated neutrophils in lung, following the identical procedures described in section 'TGF-β signaling induced EMT at primary site'. RT-qPCR primers used were listed from 5′ to 3′ as follows: *Mmp9* forward: GTGGTTCAGTTGTGGTGGTG, and reverse: CCCGCTGTATAGCTACCTCG; *Vegfa* forward: AACGATGAAGCCCTGGAGTG, and reverse: TGAGAGGTCTGGTTCCCGA; *Tnf* forward: GAAAGCATGATCCGAGATGTGGAA, and reverse: CAGTAGACAGAAGAGCGTGGTGGC; *Prok2* forward: TGCTACTTCTGCTGCTACC, and reverse: CCGCACTGAGAGTCCTTGTC.

For *In Vitro* Killing Assay, Luciferase labelled 4T1 cells (1×10^5 $well^{-1}$) were seeded in a 24-well plate. The obtained infiltrated

neutrophils on day 14, 21, and 28 were added to each well at a cell number of 1×10^6. The mixture was subsequently cultured for 24 h in incubator. Then, luciferase activity was measured using the Firefly Luciferase Reporter Gene Assay Kit (RG005, Beyotime) to determine the cellular viability of 4T1 tumor cells. Cell killing % = (1- [luminescence of samples with neutrophils] / [luminescence of samples without neutrophils]) × 100%.

2.6. Evaluation of the metastasis-inhibiting efficacy of SB525334 in vivo

Mice bearing 4T1 spontaneous lung metastasis were randomly divided into four groups receiving *i.v.* injection of saline and SB525334 at the dosage of 1 mg kg^{-1}, 5 mg kg^{-1}, and 10 mg kg^{-1} every other day. On day 28, the mice were sacrificed, and the harvested lungs were subjected to the H&E staining analysis to determine the metastasis-inhibiting efficacy. The metastasis index was calculated by ImageJ. The relative metastatic niche areas = The area of the metastatic niche / The area of the total lung. All the groups were normalized to the group receiving saline. The heart valves and small intestine were also collected and stained by H&E to study the toxicities of SB525334.

2.7. Isolation of bone marrow neutrophils

6-to-10-week-old female ICR mice were sacrificed. The femurs and tibias were harvested and immersed in 5 mL of ethanol for 10 min to sterilize. And then the sterilized femurs and tibias were washed by PBS thrice and dissected by scissors and tweezers to get rid of the muscle and fat tissues. Following that, ends of each femur and tibia were clipped carefully to expose the bone marrow, which was subsequently flushed out using RPMI 1640 *via* a syringe with 27-G needle. The obtained bone marrow eluates were filtrated through a 70-μm nylon cell strainer (352350, Falcon) to remove cell clumps and bone residuals followed by centrifugation (1000 rpm, 5 min). The supernatant was removed carefully, and the pellet was re-dispersed into 3 mL of red blood cell lysis buffer. Then the resulted mixture was centrifuged (1000 rpm, 5 min). The obtained cell pellet was re-dispersed into 2 mL of RPMI 1640 medium. Percoll gradients were prepared by layering 2 mL each of the 62%, and 55% Percoll solutions successively on top of 2 mL of 75% Percoll solution in a conical 15-mL polypropylene tube. The bone marrow cell suspension was carefully layered on the top of 55% Percoll layer followed by centrifugation (1000 *g*, 30 min), and the cell band located between 75% and 62% Percoll layer was collected and washed triple by PBS.

2.8. Preparation and characterization of SBLP

To prepare SBLP, 120 mg of Soya bean lecithin (SPC), 10 mg of $LG2C_{14}$ [27,28], 15 mg of Cholesterol and 5 mg of SB525334 were co-dissolved into 5 mL of mixed solvent ($CHCl_3$:MeOH = 3:2, v:v). The obtained mixture was subjected to rotation vacuum evaporation at 40 °C to yield a thin lipid film, which was placed under vacuum overnight to remove trace organic solvent. The lipid film was then hydrated with 5 mL of deionized water, sonicated by the ultrasonic sonicator (30%, 15 min), and extruded through the filter membranes with a pore size of 0.22 μm. The particle size and zeta potential of SBLP with a corresponding polydispersity index (PDI) were determined by dynamic laser scattering (DLS) using a ZetaPALS (Brookhaven, USA). The SBLP solution was dropped onto the carbon-membrane-coated copper mesh and dried. Then the copper mesh was observed by the transmission electron microscope (Hitachi, Japan) at an accelerating voltage of 80 kV. The release of SB525334 from liposomes was investigated using a dialysis tube. 1 mL of the liposomes was added into a dialysis tube (10 K MWCO) against 50 mL of RPMI 1640 and 4T1 TCM containing Tween 80 (1%, w:v), and gently shaken at 50 rpm and 37 °C. At predetermined time intervals, 1 mL of sample was withdrawn and filtered through a 0.22 pore-sized polycarbonate membrane filter, followed by replacing with 1 mL of fresh buffer solution with the same pH value. The amount of SB525334 released was determined by HPLC.

2.9. Fabrication and characterization of SBLP/NE

Briefly, the obtained bone marrow neutrophils (1×10^6 cell mL^{-1}) were co-incubated with SBLP (SB525334 concentration: 100 μg mL^{-1}) in RPMI 1640 medium at 37 °C for 40 min. The mixture was then centrifuged (1000 rpm, 5 min) and washed thrice with PBS to get the final product, SBLP/NE. To quantify the amount of SB525334 in SBLP/NE, SBLP/NE was lysed by RIPA Lysis Buffer (P0013B, Beyotime). An aliquot of cell lysate (100 μL) was collected and mixed with 900 μL of acetonitrile, which was vortexed for 5 min and centrifuged at 10,000 *g* for 10 min. ~20 μl of supernatant was injected into the High Performance Liquid Chromatography (HPLC, C18 column, acetonitrile:0.1% phosphoric acid at a volume ratio of 70:30, 1 mL min^{-1}) system for quantification with a detection wavelength of 330 nm. The preparation of Cou6-LP/NE followed almost the identical procedures, except Cou6-LP was used instead.

The cellular viability of prepared neutrophil cyto-pharmaceuticals was measured by Calcein AM Cell Viability Assay Kit (C2013M, CCK-F, Beyotime) according to the manufacturer's instructions. The prepared neutrophil cyto-pharmaceuticals were stained by Alexa Fluor 647-conjugated $CD11b^+$ antibody (301319, 20 ng mL^{-1}, BioLegend) and FITC-conjugated CD62L antibody (304838, 250 ng mL^{-1}, BioLegend) for FACS analysis.

To measure the migration capacity of neutrophils or neutrophil cyto-pharmaceuticals towards tumor, a Transwell chamber with 3-μm pore size (MCSP24H48, Millipore) was used. The chambers were placed on a 24-well plate with each well containing 0.8 mL of completed RPMI 1640 medium or 4T1 tumor conditioned medium (TCM). Then 10^6 neutrophils or prepared neutrophil cyto-pharmaceuticals were placed into the upper chamber, which was then incubated at 37 °C for 8 h. At the end of incubation, the lower chamber was imaged by an optical microscope (Ts2R, Nikon) and the number of migrated cells was analyzed by ImageJ. Relative migrated cells = The average number of cells in the lower chamber / the total number of feeding cells, all the groups were normalized to the migration of NE towards RPMI 1640 medium.

To determine the tumor-triggered release of SB525334 from SBLP/NE, neutrophil cyto-pharmaceuticals (1×10^6 cells) in RPMI 1640 medium or 4T1 TCM were added into a 24-well plate and then incubated at 37 °C. At different incubation time (0, 1, 3, 5, and 7 h), the supernatant was collected and analyzed by HPLC to determine the content of released SB525334. To further visualize the release of drugs from neutrophil cyto-pharmaceuticals, Cou6-LP/NE or SBLP/NE (1×10^6 cells) in 4T1 TCM or 1640 medium was incubated at 37 °C for 4 h, and then stained with Hoechst 33324 (C1022, Beyotime) for 15 min, followed by observation with CLSM (LSM 880, ZEISS). To detect the NETosis, Anti-citrullinated Histone H3 antibody (ab5103, Abcam, 1:200 dilution) and Alexa Flour 633 labelled goat anti-rabbit secondary antibody (A21071, Invitrogen, 1:1000 dilution) was applied to label citrullinated Histone H3.

2.10. Biodistribution of neutrophil cyto-pharmaceuticals

Cell Trace™ Far Red tagged neutrophil cyto-pharmaceuticals (Cell $Trace^+$ SBLP/NE) were prepared following the manufacturer's instructions (C34564, Invitrogen, ThermoFisher) and then intravenously injected into mice bearing 4T1 spontaneous lung metastasis on day 21. After 4, 12, and 24 h post-injection, tumors and lungs were collected and digested into single-cell suspensions, which were then subjected to FACS analysis. Neutrophil targeting efficiency (%) = The numbers of neutrophil cyto-pharmaceuticals in the lung or tumor (namely Cell $Trace^+$ cells) / The number of total intravenously injected neutrophil cyto-pharmaceuticals (6×10^6 cells). Besides, Cou6, Cou6-LP and Cou6-LP/NE at the same dosage of Cou6 were intravenously injected into mice

bearing 4T1 spontaneous lung metastasis on day 21. At post-injection 4, 12 and 24 h, tumors and lungs were collected and observed by IVIS Spectrum *In Vivo* Imaging System (Perkin Elmer, USA).

2.11. Tumor-triggered drug release in vivo

To observe the *in vivo* release behavior of neutrophil cytopharmaceuticals, Cou6-LP and Cou6-LP/NE at the same dosage of Cou6 were intravenously injected into mice. At post-injection 24 h, the harvested tumors and lungs were analyzed by frozen-section examination and obversed by CLSM (LSM 880, ZEISS).

2.12. Evaluation of the metastasis suppression efficacy of SBLP/NE in vivo

Mice bearing 4T1 spontaneous lung metastasis were randomly divided into four groups receiving *i.v.* injection of saline, SB525334 (1 mg kg^{-1}), NE (3×10^8 cells kg^{-1}), SBLP (1 mg kg^{-1}) and SBLP/NE (3×10^8 cells kg^{-1}, equivalent to 1 mg kg^{-1} SB525334) every other day. According to the average loading efficiency of SBLP/NE was calculated at 3.34 μg SB525334 per million cells, 1 mg kg^{-1} SB525334 approximately equals (10^6 cells × 1000 μg kg) / 3.34 μg = 3×10^8 cell kg^{-1}. Tumor size was measured twice a week using calipers and the tumor volume was calculated as Volume = 1/2 × Length × $(\text{Width})^2$. The body weights and survival periods of the mice were monitored during treatments. On day 28, the mice were sacrificed, and the harvested lungs were subjected to the H&E analysis as well as IVIS Spectrum *In Vivo* Imaging System (Perkin Elmer, USA) to determine the metastasis-inhibiting efficacy. The metastasis index was calculated by ImageJ. The relative metastatic niche areas = The areas of the metastatic niche / The area of the total lung. All the groups were normalized to group receiving saline.

To determine the EMT-inhibiting capacity of the formulations, the tumor harvested on day 28 was subjected to the immunohistochemistry analyses, conducted under the identical protocols described in section 'Evaluation of TGF-β induced EMT at primary site'. The anti-tumor responses of infiltrated neutrophils in lung collected from mice treated with different formulations on day 28 were evaluated following the identical procedures described in section 'Detection of the anti-tumor responses of infiltrated neutrophils in metastatic niche'.

2.13. Biosafety studies of SBLP/NE in vivo

Blood samples were collected from mice receiving different treatments on day 28, which were immediately placed under 25 °C for 2 h and then centrifuged at 10,000 rpm for 10 min. The serum was carefully collected and stored at −80 °C until further analysis. The levels of the inflammatory cytokines, TNF-α (E-EL-M0049c, Elabscience), IL-6 (E-EL-M0044c, Elabscience), and IL-1β (E-EL-M0037c, Elabscience), were determined by enzyme-linked immunosorbent assays (ELISA). Corresponding serum samples were diluted where necessary, ran in duplicate, and the ELISA was performed according to the assay protocol. The optical density of each well was determined using a microplate reader at 450 nm. The results were presented as picograms per milliliter. The heart valves and small intestine were collected from mice receiving different treatments on day 28 and stained by H&E to study the toxicities of different formulations.

2.14. Statistical analysis

The Student's *t*-test was applied for comparisons between two groups, one-way ANOVA test with Tukey's correction was used for comparisons of multiple groups, and a log-rank (Mantel-Cox) test was used to analyze the statistical significance in the survival analysis. Differences were considered significant when $p < 0.05$.

3. Results

3.1. TGF-β promoted dissemination of 4T1 breast tumor cells from primary site by inducing EMT

It has been well documented that TGF-β is overexpressed at primary breast tumor site [29,30]. The over-activation of TGF-β signaling in primary tumor site promotes metastasis through various pathways. In particular, TGF-β signaling is transduced through the activation of TGF-β receptor (TGF-βR) and its downstream signals subsequently activate EMT transcription factor, *Snai1* and *Twist1/2*, facilitating cancer cell dissemination [31,32]. SB525334 is a potent and selective inhibitor of TGF-β1 receptor, activin receptor-like kinase (ALK5) [33], which can inhibit the phosphorylation status of downstream Smad2/Smad3 protein (Fig. S1). As evidenced in the wound healing assay, the migration capacity of 4T1 tumor cells is increased when treated with TGF-β, and the usage of SB525334 restored it to the normal level (Fig. S2A and B). To further verify the role of TGF-β in regulating EMT, we performed RNA analysis for 4T1 cells receiving different treatments. We found that the expression of EMT-relevant transcription factors related to EMT, such as *Snai1,* and *Twist1/2*, were both increased significantly, and SB525334 restored the expression to the normal level (Fig. S2C). Moreover, the expression of epithelial markers (E-cadherin) and mesenchymal markers (Vimentin) in tumor cells were down- and up-regulated respectively when treated with TGF-β (Fig. S2D) while pharmacological treatment with SB525334 normalized the expression of E-cadherin and Vimentin. To further verify the EMT process induced by TGF-β *in vivo*, mice bearing 4T1 tumor were treated with SB525334. We found a significantly higher expression of E-cadherin and lower expression of Vimentin in 4T1 tumor treated with SB525334 (Fig. S2E and F).

3.2. TGF-β supported colonization of 4T1 breast tumor cells by dampening the anti-tumor immune response of neutrophils at metastatic niche

Based on the metastasis-supporting role of TGF-β at the primary site, we next explored the role of TGF-β at the metastatic niche, which currently remains largely unexplored. To closely mimic the *in vivo* metastatic cascades, 1×10^6 4T1-Luc cells were injected into mammary fat pad, and corresponding analysis were performed at predetermined time intervals (Fig. 2A). As suggested in Fig. 2B, 4T1 cells began to metastasize from primary tumor to lung after 14 days in a time-dependent manner. We measured the content of TGF-β in lung by enzyme-linked immunosorbent assay (ELISA) and found that the concentration of TGF-β in lung improved by around two times after 28 days when compared to day 0 (Fig. 2C). Besides, the level of TGF-β increased with the colonization and outgrowth of metastatic tumor cells in the lung. Since TGF-β is a main immune-regulatory factor and can regulate the function of immune cells [9,34], we then explored whether the elevated TGF-β at metastatic niche orchestrated the immunosuppressive microenvironment. To begin with, we characterized the phenotype of infiltrated neutrophils during metastasis progression, which is a principal immune cell at the metastatic niche [35–38]. Intriguingly, we found that more and more neutrophils ($CD11b^+Ly6G^+$, Fig. S3) migrated into lung with the progression of lung metastasis (Fig. 2D). Moreover, the infiltrated neutrophils were in proximity to colonized 4T1 cells (Fig. 2E). Next, the metastatic lungs from SB525334 treated mice were harvested and subjected to density gradient centrifugation to yield the infiltrated neutrophils for further analyses. As demonstrated in Fig. 2F, the expression of CD11b on infiltrated neutrophils, an activation marker of neutrophils [39,40], was gradually decreased with the progression of lung metastasis. The lower activated status suggested a pro-tumor phenotype of infiltrated neutrophils. Along with this line, we did the Quantitative Real-time Reverse Transcription-Polymerase Chain Reaction (qPCR) to measure the gene expression of infiltrated neutrophils associated with tumor progression (Fig. 2G). We

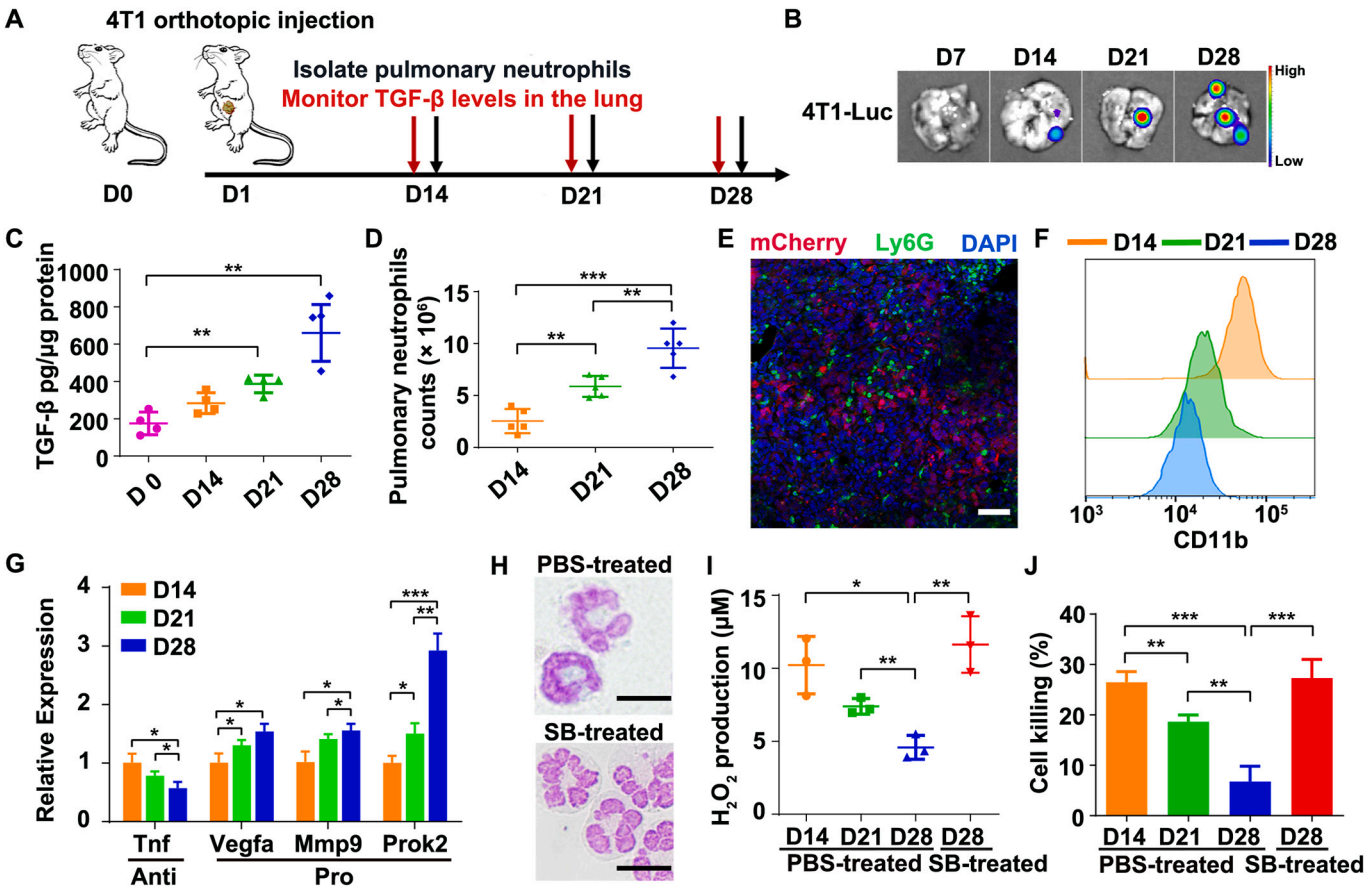

Fig. 2. TGF-β supported colonization of 4T1 breast tumor cells by dampening the anti-tumor immune response of neutrophils at the metastatic niche. (A) Schematic illustration of the experimental setup. (B) *Ex vivo* bioluminescent images of lungs harvested from mice bearing Luciferase-labelled 4T1 (4T1-Luc) tumor. (C) TGF-β levels in lungs of mice at different times detected by ELISA ($n = 4$ per group). (D) The number of infiltrated neutrophils at the metastatic niche ($n = 5$ per group). (E) A representative immunofluorescent image of the pulmonary metastatic niche on day 21 (two independent experiments). Scale bar, 50 μm. (F) The expression of CD11b on infiltrated neutrophils at different stages of metastasis. (two independent experiments). (G) The relative mRNA expression associated with phenotype of infiltrated neutrophils ($n = 3$ per group). (H) The morphology of infiltrated neutrophils at the metastatic niche on day 28. Scale bar, 20 μm. (I) H_2O_2 production in PMA-activated infiltrated neutrophils (per 0.5 million, n = 3 per group). (J) The cytotoxicity of infiltrated neutrophils towards 4T1-Luc cells by incubating isolated neutrophils with 4T1-Luc *in vitro* (4T1:NE = 1:10, n = 3 per group). Data were presented as mean ± SD and analyzed by one-way ANOVA test with Tukey's correction. $^*p < 0.05$, $^{**}p < 0.01$, $^{***}p < 0.001$.

found that the anti-tumor neutrophil marker [34,41], the *Tnf* gene, was gradually downregulated with the progression of metastasis. In contrary, the expressions of pro-tumor neutrophil markers [34,41], the *Vegfa*, *Mmp9* and *Prok2* genes, were enhanced.

We then checked whether the dampened anti-tumor immuno-responses of infiltrated neutrophils were caused by TGF-β. To this end, we pharmacologically blocked the TGF-β pathway *in vivo* by systemic injection of SB525334. As evidenced in Fig. 2H, the infiltrated neutrophils displayed a premature morphology with banded and ring-shaped nuclei (PBS-treated), while most of the neutrophils in the SB525334-treated lungs were more lobulated and hypersegmented (SB-treated), which indicated that neutrophils from SB-treated group tended to be more mature and more cytotoxic to tumor cells [34]. Moreover, the production of the main effector agent, namely hydrogen peroxide (H_2O_2), by infiltrated neutrophils significantly decreased and the overall anti-tumor efficacy consequently diminished (Fig. 2I and J). On the contrast, the administration of SB525334 significantly unleashed the anti-tumor responses of infiltrated neutrophils. Additionally, we found SB525334 displayed minimum effect on the mobilization of neutrophils into the metastatic niche, as suggested by the unchanged number of infiltrated neutrophils, ~10 million, in comparison with that in untreated mice (Fig. S4). Thereby, it is suggested that the dampened anti-tumor response was in correlation with the elevated TGF-β level at the metastatic niche, and using the TGF-β inhibitor, SB525334 could unleash the anti-tumor function of infiltrated neutrophils.

3.3. Pharmacologic blockade of TGF-β by SB525334 reduced metastasis in vivo in a dosage-dependent manner

TGF-β has been demonstrated to involve in the initial and last steps of metastasis, *i.e.* dissemination and colonization. We next sought to verify whether blockage of TGF-β could inhibit breast tumor lung metastasis. To this end, mice bearing spontaneous 4T1 lung metastasis were randomly divided into four groups, treated with saline or SB525334 with a dosage from 1 to 10 mg kg^{-1}. We found that the metastasis-inhibiting efficacy of SB525334 was in a dose-dependent manner. Mice treated with saline suffered the severest lung metastasis, and the administration of SB525334 (1 mg kg^{-1}) moderately suppressed the metastasis (Fig. 3A and B). The improved or even complete suppression was achieved when a higher dosage (5 and 10 mg kg^{-1}) was administered. We then examined toxicities of SB525334 towards the heart and small intestine, which were the main toxicity-related organs reported by other groups [15–17]. As displayed in Fig. 3C, the valve and vascular endothelial cells were heavily injured and inflamed indicted by the increased vascular permeability and infiltrated inflammatory cells, showing pathological proliferation of fibrous cells under all dosages. Moreover, we found the distortion of crypt architecture and pathological proliferation of lymphoid tissues in the small intestine under a dosage of

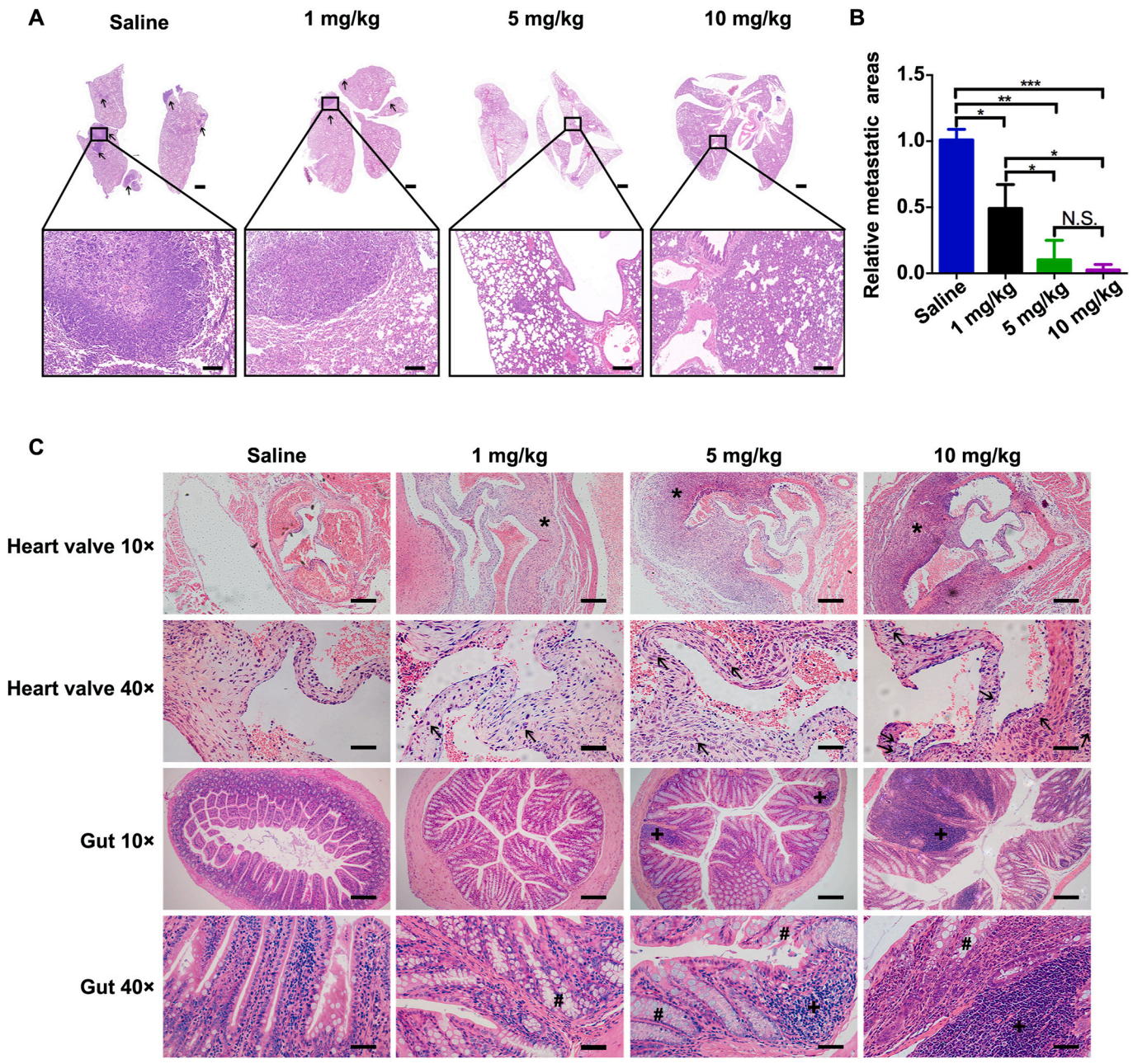

Fig. 3. The bio-performance of TGF-β inhibitor *in vivo*. (A) Represntative images of hematoxylin-eosin (H&E) stained lungs collected from 4T1 tumor-bearing mice treated with saline or SB525334 (1, 5, and 10 mg kg^{-1}), Scale bar, 1 mm (upper); 200 μm (lower). (B) Quantified relative metastatic niche areas from each group compared to saline group ($n = 3$ per group). Data were presented as mean ± SEM and analyzed by one-way ANOVA test with Tukey's correction. $^{*}p < 0.05$, $^{**}p < 0.01$, $^{***}p < 0.001$. (C) Representative images of H&E stained heart valves as well as small intestines collected from 4T1 tumor-bearing mice treated with saline or SB525334 (1, 5, and 10 mg kg^{-1}, n = 3 per group). Black arrows indicated inflammatory cells infiltration; Asterisks (*) indicated vascular wall thickening; Hashes (#) indicated distortion of crypt architecture; Plus signs (+) indicated pathological proliferation of lymphoid tissues. Scale bar, 200 μm (10×); 50 μm (40×).

5 or 10 mg kg^{-1}. Despite the great potential of SB525334 held as a metastasis-directed metastasis-inhibiting agent, the severe toxicities limited the *in vivo* application [14]. A targeted drug delivery system might improve the therapeutic index.

3.4. Fabrication and characterization of neutrophil cyto-pharmaceuticals of SB525334

Neutrophils, as the most abundant leukocytes in circulation [26], can migrate into primary tumor [26,42] as well as metastasis sites [35,36]. In an effort to achieve an improved therapeutic index of SB525334, we chose neutrophils as the carrier to fabricate neutrophil cyto-pharmaceutical of SB525334 (Fig. 4A). To this end, we first prepared liposomal SB525334 (SBLP) as previously reported [23]. The prepared SBLP displayed an average particle size of 60 nm and a zeta potential of about +20 mV (Fig. S5) and a sustained release of SB525334 was achieved by liposomal encapsulation (Fig. S6). The SBLP was subsequently co-incubated with neutrophils to yield neutrophil cyto-pharmaceuticals of SB525334 (SBLP/NE). To verify the location of SBLP in SBLP/NE, liposome was tagged by coumarin-6 (Cou6-LP/NE). As shown in Fig. 4B, the Cou6-LP was located in the cytoplasm of neutrophils. The loading efficiency of SBLP/NE was calculated at 3.34 μg SB525334 per million cells. As displayed in Fig. 4C, since the overall cell viability had about 20% decrease after 8 h due to neutrophils' short-lived nature especially

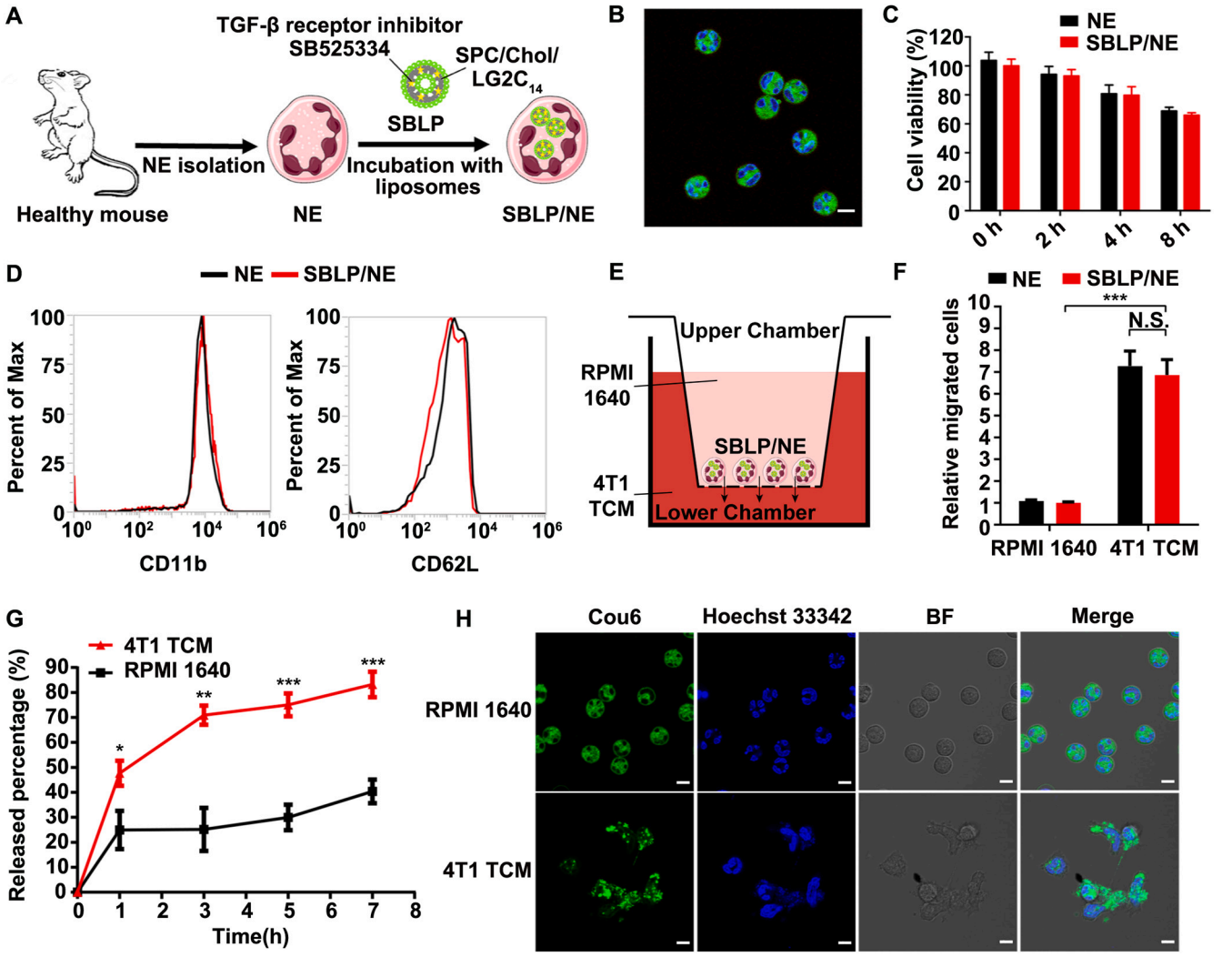

Fig. 4. Fabrication and characterization of neutrophil cyto-pharmaceuticals of SB525334. (A) Schematic illustration of preparation of neutrophil cyto-pharmaceuticals. (B) The fluorescent image of Cou6-tagged neutrophil cyto-pharmaceuticals (two independent experiments). Scale bar, 5 μm. (C) The cell viability of neutrophil cyto-pharmaceuticals *in vitro* ($n = 6$ per group). (D) The expression of CD11b and CD62L on neutrophil cyto-pharmaceuticals analyzed by the flow cytometry (two independent experiments). (E) Schematic illustration of transwell migration assay. (F) Quantification of relative migrated NE or SBLP/NE analyzed by transwell migration assay ($n = 3$ per group). (G) The release profile of neutrophil cyto-pharmaceuticals in RPMI 1640 medium or 4T1 TCM (n = 3 per group). (H) The fluorescent images of neutrophil cyto-pharmaceuticals after incubation with 4T1 TCM or RPMI 1640 medium for 4 h (two independent experiments). Scale bar, 5 μm. Data were presented as mean ± SD and analyzed by Student's *t*-test. $^{**}p < 0.01$, $^{*}p < 0.05$, $^{***}p < 0.001$.

in vitro [43], no significant reduction of cell viability of SBLP/NE was observed compared with NE, demonstrating the fabrication of neutrophil cyto-pharmaceuticals was benign. Moreover, the expression of activation markers [40], like CD11b and CD62L, on SBLP/NE maintained unperturbed as measured by the flow cytometry (Fig. 4D). The migration capacity of SBLP/NE towards tumor was measured by the Transwell assay (Fig. 4E). We found that the number of SBLP/NE migrated towards tumor conditioned medium (TCM) was nearly ten times more than those towards RPMI 1640 medium (Fig. 4F). Moreover, the migration capacity of SBLP/NE towards TCM kept intact in comparison with NE (Fig. 4F). Lastly, the release kinetics of payloads from cyto-pharmaceuticals was monitored. We found that the cyto-pharmaceuticals maintained intact in the 1640 medium up to 7 h with only 30% of the payloads leaked. While, in the TCM, the cyto-pharmaceuticals swiftly released nearly 70% of the payloads within 3 h (Fig. 4G). We also verified the tumor-triggered drug release by CLSM and found the relevant rupture of the cell membrane in the stimuli of 4T1 TCM compared with that in RPMI 1640 medium (Fig. 4H). Since 4T1 cells can induce neutrophil extracellular traps (NETs) by secreting cytokines like G-CSF [42] and the process of NET involves the rupture of the cell membrane [44], we further stained the NETs with citrullinated Histone H3 and found that the 4T1-TCM-specific drug release was in connection with the NETosis of the cyto-pharmaceuticals. (Fig. S7). Overall, this tumor-triggered drug release behavior of cyto-pharmaceuticals was favorable for the biocompatibility of tumor-targeted drug delivery.

3.5. *In vivo behavior of neutrophil cyto-pharmaceuticals*

Encouraged by the superior *in vitro* behavior of neutrophil cyto-pharmaceuticals, we next investigated their *in vivo* behavior after a systemic infusion into mice bearing 4T1 spontaneous lung metastasis. To evaluate the spontaneous migration of neutrophil cyto-pharmaceuticals *in vivo*, we labelled SBLP/NE with Cell Trace™ Far Red (Cell Trace$^+$ SBLP/NE), and analyzed the frequency of Cell Trace$^+$ SBLP/NE the metastatic niche and primary tumor (Fig. 5A). As displayed in Fig. S8, the Cell Trace$^+$ SBLP/NE, simultaneously accumulated into lung and tumor in a time-dependent manner. We calculated the corresponding neutrophil targeting efficiency and found that at 12 h post-infusion, the total targeting efficiency (both tumor and lung) reached a plateau at

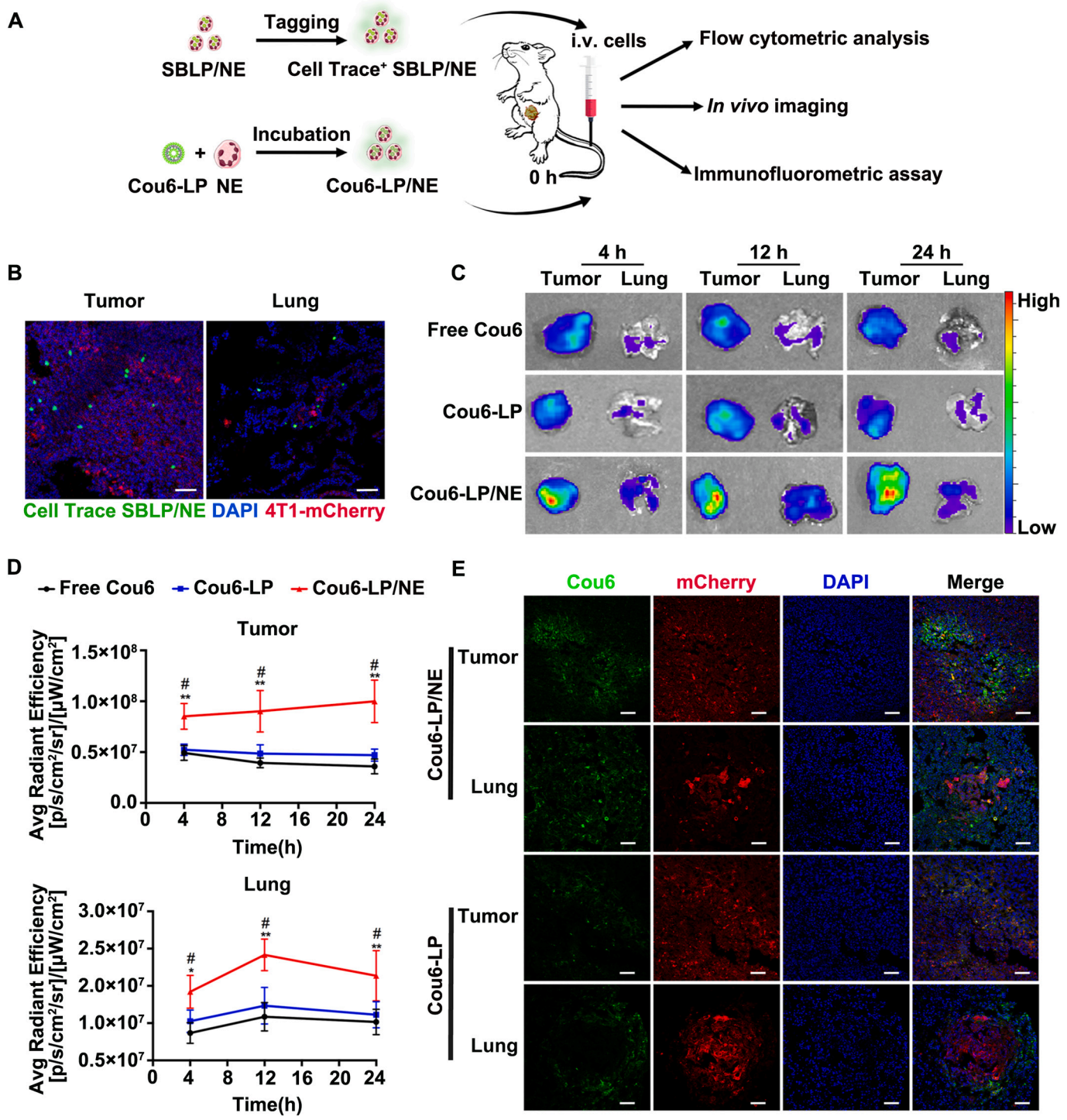

Fig. 5. *In vivo* behavior of infused neutrophil cyto-pharmaceuticals in mice bearing 4T1 spontaneous lung metastasis. (A) Schematic illustration of the experimental setup. (B) The typical fluorescent images of infused cyto-pharmaceuticals in primary tumor and metastatic niche (two independent experiments). Scale bar, 100 μm. (C) *Ex vivo* fluorescent images of the tumor and lung collected from mice receiving Cou-6, Cou6-LP, or Cou6-LP/NE, at 4, 12, and 24 h post-injection. (D) Quantified fluorescence intensity of the tumor and lung collected from mice receiving Cou-6, Cou6-LP, or Cou6-LP/NE, at 4, 12, and 24 h post-injection ($n = 3$ per group). Data were presented as mean ± SEM and analyzed by one-way ANOVA test with Tukey's correction. $^{*}p < 0.05$ (free Cou6 *vs* Cou6-LP/NE), $^{**}p < 0.01$, $^{\#}p < 0.05$ (Cou6-LP *vs* Cou6-LP/NE). (E) The typical fluorescent images of the primary tumor and metastatic niche (lung) harvested from mice treated with Cou6-LP and Cou6-LP/NE (two independent experiments). Scale bar, 50 μm.

approximately 4.48%. The fluorescent images of frozen sections of lung and primary tumor further verified the simultaneous infiltration of neutrophils into primary tumor and metastatic niche (Fig. 5B).

We next investigated whether neutrophil cyto-pharmaceuticals could convey their payloads into the two sites of interest. To make the payloads observable, we used the Cou6 instead. As suggested in Fig. 5C, D, and Fig. S9, Cou6-LP/NE conveyed the most payloads into the tumor, followed by Cou6-LP at 24 h post injection. The free Cou6 displayed minimum accumulation in tumor. Such an accumulation pattern of Cou6 for all groups was also observed in lung, except for a peak-reaching time

of ~12 h. Lastly, we investigated the release of payloads from accumulated Cou6-LP/NE at primary and metastatic sites (Fig. 5E). The fluorescent signal of Cou6 in the Cou6-LP/NE group (Green) well co-localized with lung metastasis regions (Red) indicating that Cou6-LP/NE released Cou6-LP which was then internalized by tumor cells (Fig. S10). At the same time, the fluorescent signal of Cou6 in the Cou6-LP group was rare in lung metastasis regions and most Cou6 (Green) were accumulated at the edge of the lung metastasis regions (Red) probably due to the lower accumulation and penetration of Cou6-LP in lung metastasis regions compared with Cou6-LP/NE. Similarly, this tumor-triggered drug release behavior was also observed at primary site, demonstrated by the superior green signals of Cou6 inside tumor in the Cou6-LP/NE group than that in the Cou6-LP group.

All in all, neutrophil cyto-pharmaceuticals could simultaneously accumulate into both metastatic niche and primary tumor, and then release their payloads in response to tumor stimuli.

3.6. *In vivo metastasis-inhibiting efficacy of neutrophil cyto-pharmaceuticals*

Inspired by the substantial targeting and releasing behavior of SBLP/NE *in vivo*, we next investigated the metastasis suppression efficacy of SBLP/NE. As displayed in Fig. 6A, mice bearing spontaneous lung metastasis of 4T1 breast tumor were randomly divided into four groups, and further treated with saline, blank NE (3×10^8 cells kg^{-1}), SB525334 (1 mg kg^{-1}), SBLP (1 mg kg^{-1}), and SBLP/NE (3×10^8 cells kg^{-1}, equivalent to 1 mg kg^{-1} SB525334). After receiving several treatments, the mice were sacrificed for further analysis. The harvested lungs from all groups were subjected to the Living Animal Imaging System. We found that metastasis in mice receiving SBLP/NE was significantly suppressed. SB525334 and SBLP showed moderate metastatic-inhibiting efficacy. Notably, the administration of NE did not inhibit lung metastasis (Fig. 6B and C). The immune-histological staining of harvested lungs further confirmed the superior metastasis-inhibiting efficacy of SBLP/NE (Fig. 6D and E). Moreover, mice receiving saline, NE, SB525334, and SBLP/NE survived no more than 55 days, while approximately 50% of mice treated with SBLP/NE survived on day 55 (Fig. 6F). However, there were no mice in all groups survived eventually. It was possible that the burden of the primary tumor attributed to the sacrifice of mice treated with SBLP/NE despite its successful treatment on metastasis, since we did not observe a significant reduction of primary tumor volume when treated with SB525334, SBLP or SBLP/NE (Fig. S11).

We hypothesized the superior metastasis-inhibiting efficacy of SBLP/NE was attributed to the inhibition of EMT at the primary site and recovery of anti-tumor capacity of infiltrated neutrophils at metastatic niche. To verify this, the harvested primary tumor was immune-histologically stained. As evidenced by Fig. 6G and H, the EMT process was significantly blocked in mice administrated with SBLP/NE, which was indicated by the least Vimentin and most E-cadherin expression at the primary site. In the primary tumors of mice receiving SBLP, the EMT process was moderately inhibited, followed by SB525334. The slightly stronger EMT-inhibiting capacity of SBLP than SB525334 in the primary site was likely due to the higher concentration of SB525334 in primary tumor delivered by liposome (Fig. 5D). Administration of NE did not suppress the EMT. Additionally, we isolated the infiltrated neutrophils at metastatic niche by density gradient centrifugation. As displayed in Fig. 6I and J, the capacity to produce the main effector agent by infiltrated neutrophils, *i.e.* H_2O_2 and TNF-α, from mice receiving SBLP/NE both significantly recovered, which consequently improved the overall tumor-killing ability (Fig. 6K, $p = 0.0005$). Contrarily, the genes associated with pro-tumor effects in infiltrated neutrophils, such as *Vegfa*, *Mmp9,* and *Prok2*, were all strikingly down-regulated (Fig. 6L). For mice receiving SB525334, the capacity to produce anti-tumor agents, including H_2O_2 and TNF-α, by infiltrated neutrophils was both significantly improved with a moderate tumor-killing potential ($p = 0.0076$). The expression of genes regarding the pro-tumor effects, such as *Mmp9* and *Prok2*, was significantly lowered. Similarly, infiltrated neutrophils from mice receiving SBLP, displayed a moderate anti-tumor phenotype ($p = 0.003$), with an improved expression of H_2O_2 and down-regulated expressions of *Vegfa*, *Mmp9,* and *Prok2*.

3.7. *The preclinical biosafety profiles of neutrophil cyto-pharmaceuticals*

Considering the immune cell used in SBLP/NE, namely neutrophils, we first investigated whether the systemic infusion of SBLP/NE would evoke an inflammatory cytokine storm by measuring the serum levels of pro-inflammatory cytokines, including TNF-α, IL-1β, and IL-6, in mice receiving different formulations. As suggested in Fig. 7A-C, no significant increases were observed from the level of these cytokines after systemic infusion of SBLP/NE, indicating no inflammatory storm happened during treatment. Next, the harvested hearts and intestines from mice receiving different treatments were analyzed by H&E staining. We found that administration of neither SBLP or SBLP/NE induced observable toxicities towards hearts and intestines, which might stem from the targeted delivery of SB525334 by the carriers, *i.e.* liposomes and neutrophils (Fig. 7D). Moreover, the functional indexes of the liver (such as alanine transaminase (ALT) and aspartate transaminase (AST)), and renal functional biomarkers (such as blood urea nitrogen (BUN) and creatinine (CRE)) in mice receiving SBLP/NE were normal, demonstrating no acute toxicities of SBLP/NE to mice (Fig. 7E and F). Taken together, the safety of SBLP/NE treatment was satisfactory without any detectable toxicities.

4. Discussion

It has been well established that TGF-β participates in the dissemination step of metastasis by inducing EMT, which facilitates the intravasation of tumor cells into the blood vessels [45–47]. However, the metastasis-promoting puzzle of TGF-β in metastatic niche remains to be explored, particularly in lung metastasis. Herein, we verify that the levels of TGF-β in the lungs of tumor-bearing mice increase accordingly with metastatic progression. In view that neutrophils are the major immune component in metastatic lung and their cytotoxicity is blocked by TGF-β in the primary tumor microenvironment [34], we discovered that high expression of TGF-β at the metastatic site can induce pro-tumor phenotype of lung neutrophils. Correspondingly, blockade of TGF-β recovered the anti-tumor responses of neutrophils with higher expressions of metastasis-inhibiting-associated genes.

Based on the contextual roles of TGF-β played in the breast tumor lung metastasis cascades, we verify the metastasis suppression efficacy of TGF-β inhibitor, SB525334, *in vivo*. However, the toxicities of SB525334 to the heart and small intestine retard the therapeutic benefits. Cyto-pharmaceuticals, which can specifically deliver drugs to sites of interest without non-specific distribution [23,48], are thereby attractive. Based on the superior tropism of neutrophils towards primary and metastatic tumor cells, a neutrophil cyto-pharmaceutical of SB525334 was fabricated on the basis of our previous reports to improve the therapeutic index. As expected, our neutrophil cyto-pharmaceuticals enable TGF-β inhibitor to exert their full anti-metastasis potential at the target sites by interrupting the EMT process at the primary site and enhancing the anti-tumor capacity of infiltrated neutrophils at metastatic niche respectively. It is well known that TGF-β can polarize many arms of the immune system [9,49], including the phenotype of tumor-associated neutrophils [34]. Besides, previous studies showed that factors derived from neutrophils isolated from metastatic lungs, like leukotrienes, IL-6, MMP9, could favor metastatic cell colonization [35,36,38]. Our neutrophil cyto-pharmaceuticals unleashed the anti-tumor immune response of these neutrophils in lung metastatic with enhanced cytotoxicity towards tumor cells and depressed pro-tumor gene expressions like *Mmp9* and *Vegfa*. On the other hand, our cyto-

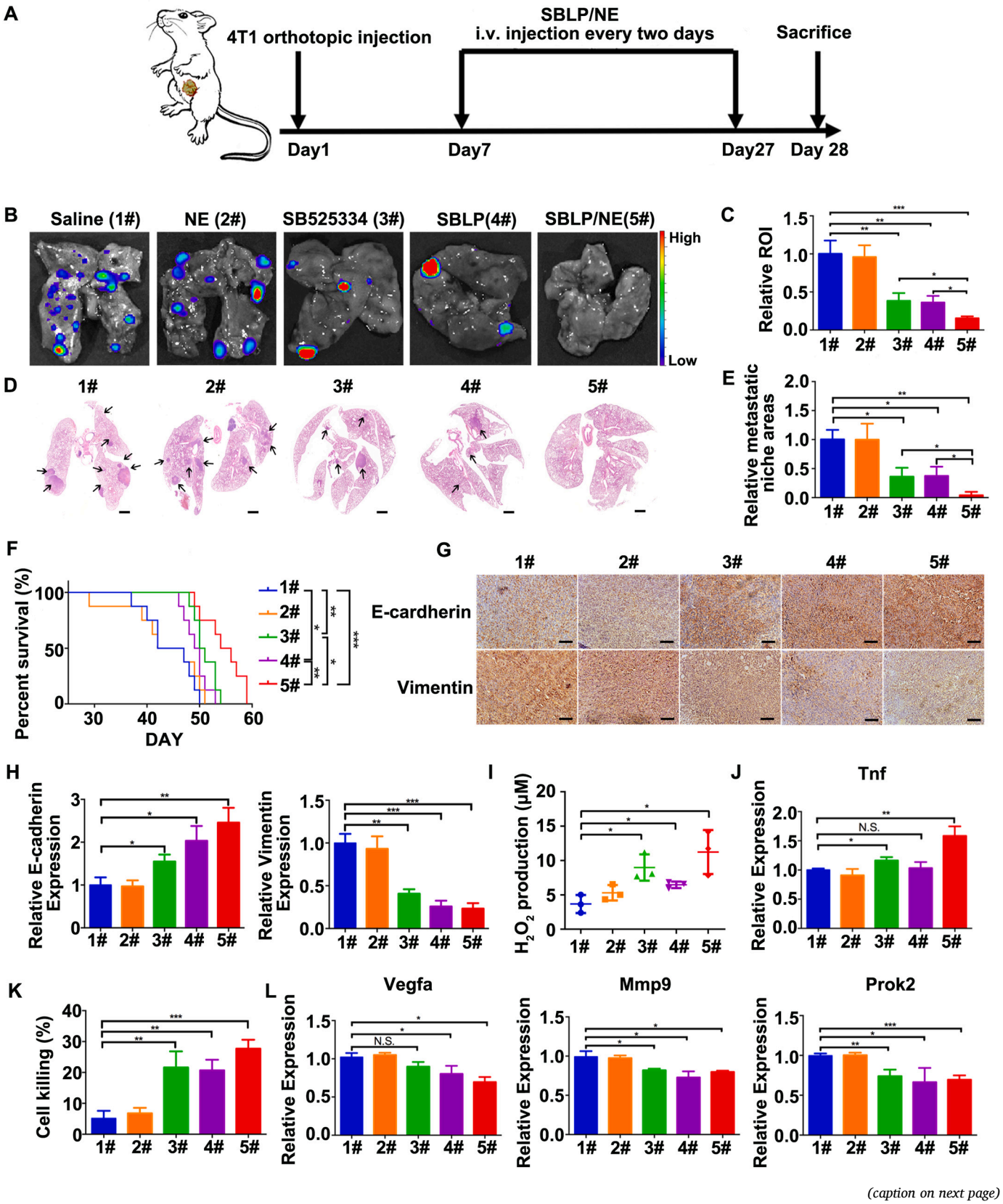

(caption on next page)

Fig. 6. *In vivo* metastasis-inhibiting efficacy of neutrophil cyto-pharmaceuticals. (A) Schematic illustration of the experimental setup. (B) Representative *ex vivo* fluorescent images collected from mice on day 28. 1#, 2#, 3#, 4#, and 5# represent the group of Saline, NE, SB525334, SBLP, and SBLP/NE respectively. (C) Quantified relative fluorescence intensity of lungs from each group compared to saline group (n = 5 per group). Data were presented as mean ± SEM. (D) Representative images of H&E stained lungs collected from mice on day 28. Scale bar, 1 mm. (E) Quantified relative metastatic niche areas of lungs from each group compared to saline group (n = 5 per group). Data were presented as mean ± SEM. (F) Survival curves of 4T1-bearing mice receiving different treatments (n = 8 per group). Data were presented as mean ± SEM. (G) Immunohistochemistry analysis of E-cadherin and Vimentin expression in primary tumor. Scale bar, 100 μm. (H) Quantified relative E-cadherin and Vimentin expression of in primary tumor collected from mice receiving different treatments (n = 3 per group). (I) H_2O_2 production in PMA-activated infiltrated neutrophils (per 0.5 million) in metastatic niche after receiving different treatments (n = 5 per group). (J) The relative TNFα mRNA (*Tnf*) expression of infiltrated neutrophils (n = 3 per group). (K) The cytotoxicity of infiltrated neutrophils towards 4T1-Luc cells by incubating isolated neutrophils with 4T1-Luc *in vitro* (4T1:NE = 1:10, n = 3 per group). (L) The relative mRNA expression associated with pro-tumor function of infiltrated neutrophils (n = 3 per group). Data were presented as mean ± SD. Data were analyzed by one-way ANOVA with Tukey's correction (C, E, and H to L) or a Log-rank (Mantel–Cox) test (F). $^{*}p < 0.05$, $^{**}p < 0.01$, $^{***}p < 0.001$.

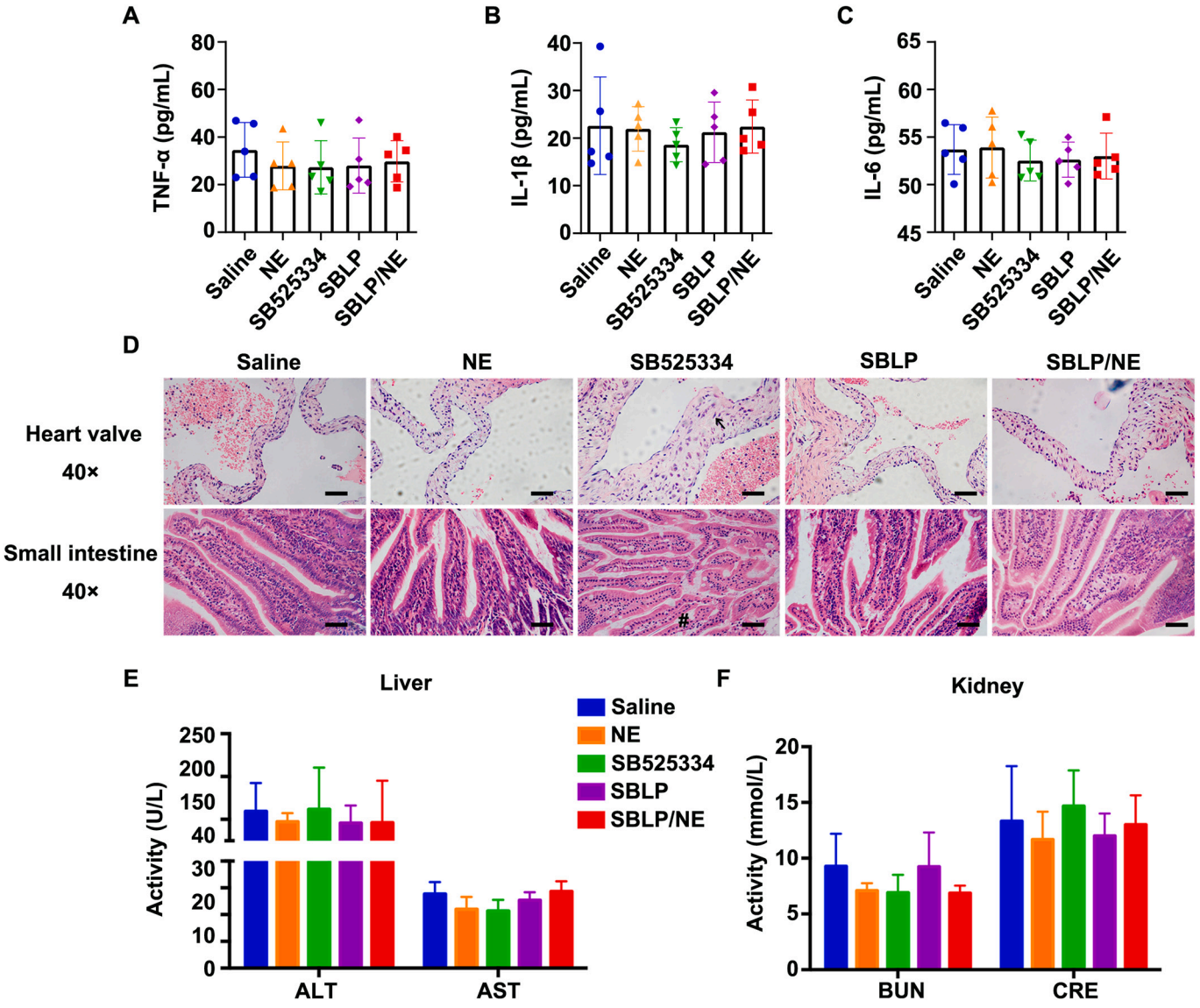

Fig. 7. The preclinical biosafety profiles of neutrophil cyto-pharmaceuticals. Serum levels of TNF-α (A), IL-1β (B), and IL-6 (C) in 4T1-bearing mice receiving different treatments (n = 5 per group). (D) H&E stained heart valves and small intestines of 4T1-bearing mice receiving different treatments. Black arrows indicated inflammatory cells infiltration; Hashes (#) indicated distortion of crypt architecture. Scale bar, 50 μm. (E), (F) Blood biochemical indexes, including AST, ALT, BUN, and CRE of 4T1-bearing mice treated with different formulations (n = 3 per group). Data were presented as mean ± SD. AST: aspartate aminotransferase. ALT: alanine aminotransferase. BUN: blood urea nitrogen. CRE: creatinine.

pharmaceuticals did not show adverse immune responses like inflammatory cytokine storm, probably due to the short-lived nature and non-proliferation ability of neutrophils.

The principal purpose of our study is to verify the metastasis-inhibiting benefits of drugs targeting metastatic cascades, so we take metastasis as the evaluating index. As for the growth of primary tumor, we did not observe a significant reduction when treated with SB, SBLP, or SBLP/NE (Fig. S11), which is in accordance with other studies [16,50]. For a future study, tumor-growth inhibiting therapy could be combined with SBLP/NE to make this therapy more clinic-relevant.

There have already been neutrophil-based therapies applied in the clinical. For example, granulocyte transfusion therapy has been applied for the treatment of granulocytopenia [51,52]. Besides, granulocyte infusion has been in the clinical trial for the anti-tumor therapies [53], although the efficacy needs to be further improved. These studies indicate that the application of neutrophil cyto-pharmaceuticals may be feasible and safe, which favors our cyto-pharmaceuticals for further clinical translation. Our group has also done some researches on human-derived neutrophils targeted therapy for cancer in the early stage [6], and is exploring more ways to improve the anti-tumor effect [24].

Taken together, TGF-β within the metastasis environment plays a significant role in modulating the phenotype of tumor-associated neutrophils. Enhancing anti-tumor effects of neutrophils to improve metastatic microenvironment and suppress metastasis colonization may reduce the metastatic risk even if the tumor cells have entered into the circulation. By blocking TGF-β signals involved in the EMT process and polarization of tumor-associated neutrophil phenotype, SBLP/NE controls both "seeding and soil" of metastasis.

5. Conclusion

In summary, TGF-β at the metastatic niche was positively related to the colonization step of metastasis by dampening the anti-tumor potential of infiltrated neutrophils. Besides, TGF-β at the primary site induced EMT to promote the dissemination of tumor cells. By simultaneous blockage of contextual TGF-β using neutrophil cyto-pharmaceutical, the 4T1 breast cancer lung metastasis was significantly suppressed. This study not only discovers the contextual roles of TGF-β in breast cancer lung metastasis but also paves a new avenue for metastasis-inhibiting therapy based on the metastatic-cascades-targeting strategy.

Author contributions

Can Zhang and Cong Wang conceived this project, and Yanyi Li and Weishuo Li designed the project. Cong Wang, Yanyi Li, Qifan Hu, Shijing Liu, Kaiming Li, Xiaoyu Li, Junjie Du and Zexuan Yu performed the experiments, and Yanyi Li, Qifan Hu and Weishuo Li analyzed the data and wrote the manuscript. Can Zhang supervised the project. All authors discussed the results and commented on the manuscript.

Declaration of Competing Interest

The authors declare no competing interests.

Acknowledgments

We thank the Public Platform of the State Key Laboratory of Natural Medicines for assistance with the pathological-section imaging. This work was supported by the National Natural Science Foundation of China (81930099, 81773664, 81473153, 81703585, 81803465), National Major Scientific and Technological Special Project for "Significant New Drugs Development" (2019ZX09301163), 111 Project from the Ministry of Education of China and the State Administration of Foreign Expert Affairs of China (No. 111-2-07, B17047), "Double First-Class" University project (CPU2018GY47, CPU2018GF10), the Open Project of State Key Laboratory of Natural Medicines (No. SKLNMZZ202017) and the Natural Science Foundation of Jiangsu Province (BK20180552).

Appendix A. Supplementary data

Supplementary data to this article can be found online at https://doi.org/10.1016/j.jconrel.2021.06.012.

References

[1] S. Valastyan, R.A. Weinberg, Tumor metastasis: molecular insights and evolving paradigms, Cell 147 (2011) 275–292, https://doi.org/10.1016/j.cell.2011.09.024.
[2] G.P. Gupta, J. Massague, Cancer metastasis: building a framework, Cell 127 (2006) 679–695, https://doi.org/10.1016/j.cell.2006.11.001.
[3] P.S. Steeg, Tumor metastasis: mechanistic insights and clinical challenges, Nat. Med. 12 (2006) 895–904, https://doi.org/10.1038/nm1469.
[4] P.S. Steeg, Targeting metastasis, Nat. Rev. Cancer 16 (2016) 201–218, https://doi.org/10.1038/nrc.2016.25.
[5] A.W. Lambert, D.R. Pattabiraman, R.A. Weinberg, Emerging biological principles of metastasis, Cell 168 (2017) 670–691, https://doi.org/10.1016/j.cell.2016.11.037.
[6] D.X. Nguyen, P.D. Bos, J. Massague, Metastasis: from dissemination to organ-specific colonization, Nat. Rev. Cancer 9 (2009) 274–284, https://doi.org/10.1038/nrc2622.
[7] J. Massague, TGFbeta in Cancer, Cell 134 (2008) 215–230, https://doi.org/10.1016/j.cell.2008.07.001.
[8] H. Ikushima, K. Miyazono, TGFβ signalling: a complex web in cancer progression, Nat. Rev. Cancer 10 (2010) 415–424, https://doi.org/10.1038/nrc2853.
[9] R.A. Flavell, S. Sanjabi, S.H. Wrzesinski, P. Licona-Limon, The polarization of immune cells in the tumour environment by TGF beta, Nat. Rev. Immunol. 10 (2010) 554–567, https://doi.org/10.1038/nri2808.
[10] J. Seoane, R.R. Gomis, TGF-beta family signaling in tumor suppression and cancer progression, Cold Spring Harb. Perspect. Biol. 9 (2017), https://doi.org/10.1101/cshperspect.a022277.
[11] M. Korpal, J. Yan, X. Lu, S. Xu, D.A. Lerit, Y. Kang, Imaging transforming growth factor-beta signaling dynamics and therapeutic response in breast cancer bone metastasis, Nat. Med. 15 (2009) 960–966, https://doi.org/10.1038/nm.1943.
[12] K.S. Mohammad, D. Javelaud, P.G. Fournier, M. Niewolna, C.R. McKenna, X. H. Peng, V. Duong, L.K. Dunn, A. Mauviel, T.A. Guise, TGF-beta-RI kinase inhibitor SD-208 reduces the development and progression of melanoma bone metastases, Cancer Res. 71 (2011) 175–184, https://doi.org/10.1158/0008-5472.CAN-10-2651.
[13] A. Bandyopadhyay, J.K. Agyin, L. Wang, Y. Tang, X. Lei, B.M. Story, J.E. Cornell, B. H. Pollock, G.R. Mundy, L.Z. Sun, Inhibition of pulmonary and skeletal metastasis by a transforming growth factor-beta type I receptor kinase inhibitor, Cancer Res. 66 (2006) 6714–6721, https://doi.org/10.1158/0008-5472.CAN-05-3565.
[14] S. Herbertz, J.S. Sawyer, A.J. Stauber, I. Gueorguieva, K.E. Driscoll, S.T. Estrem, A. L. Cleverly, D. Desaiah, S.C. Guba, K.A. Benhadji, C.A. Slapak, M.M. Lahn, Clinical development of galunisertib (LY2157299 monohydrate), a small molecule inhibitor of transforming growth factor-beta signaling pathway, Drug Des. Dev. Ther. 9 (2015) 4479–4499, https://doi.org/10.2147/DDDT.S86621.
[15] M. Sato, Y. Muragaki, S. Saika, A.B. Roberts, A. Ooshima, Targeted disruption of TGF-β1/Smad3 signaling protects against renal tubulointerstitial fibrosis induced by unilateral ureteral obstruction, J. Clin. Invest. 112 (2003) 1486–1494, https://doi.org/10.1172/jci200319270.
[16] C.J. Martin, A. Datta, C. Littlefield, A. Kalra, C. Chapron, S. Wawersik, K.B. Dagbay, C.T. Brueckner, A. Nikiforov, F.T. Danehy, F.C. Streich, C. Boston, A. Simpson, J. W. Jackson, S. Lin, N. Danek, R.R. Faucette, P. Raman, A.D. Capili, A. Buckler, G. J. Carven, T. Schurpf, Selective inhibition of TGF beta 1 activation overcomes primary resistance to checkpoint blockade therapy by altering tumor immune landscape, Sci. Transl. Med. 12 (2020), eaay8456, https://doi.org/10.1126/scitranslmed.aay8456.
[17] S. Hong, H.J. Lee, S.J. Kim, K.B. Hahm, Connection between inflammation and carcinogenesis in gastrointestinal tract: focus on TGF-beta signaling, World J. Gastroenterol. 16 (2010) 2080–2093, https://doi.org/10.3748/wjg.v16.i17.2080.
[18] T. Li, H. Dong, C. Zhang, R. Mo, Cell-based drug delivery systems for biomedical applications, Nano Res. 11 (2018) 5240–5257, https://doi.org/10.1007/s12274-018-2179-5.
[19] L.A.L. Fliervoet, E. Mastrobattista, Drug delivery with living cells, Adv. Drug Deliv. Rev. 106 (2016) 63–72, https://doi.org/10.1016/j.addr.2016.04.021.
[20] J. Jablonska, C.F. Wu, L. Andzinski, S. Leschner, S. Weiss, CXCR2-mediated tumor-associated neutrophil recruitment is regulated by IFN-beta, Int. J. Cancer 134 (2014) 1346–1358, https://doi.org/10.1002/ijc.28551.
[21] O. Florey, D.O. Haskard, Sphingosine 1-phosphate enhances fc gamma receptor-mediated neutrophil activation and recruitment under flow conditions, J. Immunol. 183 (2009) 2330–2336, https://doi.org/10.4049/jimmunol.0901019.
[22] A. Swierczak, K.A. Mouchemore, J.A. Hamilton, R.L. Anderson, Neutrophils: important contributors to tumor progression and metastasis, Cancer Metastasis Rev. 34 (2015) 735–751, https://doi.org/10.1007/s10555-015-9594-9.
[23] J. Xue, Z. Zhao, L. Zhang, L. Xue, S. Shen, Y. Wen, Z. Wei, L. Wang, L. Kong, H. Sun, Q. Ping, R. Mo, C. Zhang, Neutrophil-mediated anticancer drug delivery for suppression of postoperative malignant glioma recurrence, Nat. Nanotechnol. 12 (2017) 692–700, https://doi.org/10.1038/nnano.2017.54.
[24] C. Ju, Y. Wen, L. Zhang, Q. Wang, L. Xue, J. Shen, C. Zhang, Neoadjuvant chemotherapy based on Abraxane/human neutrophils Cytopharmaceuticals with radiotherapy for gastric Cancer, Small 15 (2019), e1804191, https://doi.org/10.1002/smll.201804191.
[25] L. Zhang, Y. Zhang, Y. Xue, Y. Wu, Q. Wang, L. Xue, Z. Su, C. Zhang, Transforming weakness into strength: photothermal-therapy-induced inflammation enhanced cytopharmaceutical chemotherapy as a combination anticancer treatment, Adv. Mater. 31 (2019), e1805936, https://doi.org/10.1002/adma.201805936.
[26] S.B. Coffelt, M.D. Wellenstein, K.E. de Visser, Neutrophils in cancer: neutral no more, Nat. Rev. Cancer 16 (2016) 431–446, https://doi.org/10.1038/nrc.2016.52.

[27] Y. Obata, D. Suzuki, S. Takeoka, Evaluation of cationic assemblies constructed with amino acid based lipids for plasmid DNA delivery, Bioconjug. Chem. 19 (2008) 1055–1063, https://doi.org/10.1021/bc700416u.
[28] D. Xie, J. Du, M. Bao, A. Zhou, C. Tian, L. Xue, C. Ju, J. Shen, C. Zhang, A one-pot modular assembly strategy for triple-play enhanced cytosolic siRNA delivery, Biomater. Sci. 7 (2019) 901–913, https://doi.org/10.1039/c8bm01454j.
[29] H. Moses, M.H. Barcellos-Hoff, TGF-beta biology in mammary development and breast cancer, Cold Spring Harb. Perspect. Biol. 3 (2011) a003277, https://doi.org/10.1101/cshperspect.a003277.
[30] Y. Kojima, A. Acar, E.N. Eaton, K.T. Mellody, C. Scheel, I. Ben-Porath, T.T. Onder, Z.C. Wang, A.L. Richardson, R.A. Weinberg, A. Orimo, Autocrine TGF- and stromal cell-derived factor-1 (SDF-1) signaling drives the evolution of tumor-promoting mammary stromal myofibroblasts, Proc. Natl. Acad. Sci. U. S. A. 107 (2010) 20009–20014, https://doi.org/10.1073/pnas.1013805107.
[31] V. Syed, TGF-beta signaling in Cancer, J. Cell. Biochem. 117 (2016) 1279–1287, https://doi.org/10.1002/jcb.25496.
[32] M.A. Nieto, R.Y. Huang, R.A. Jackson, J.P. Thiery, Emt: 2016, Cell 166 (2016) 21–45, https://doi.org/10.1016/j.cell.2016.06.028.
[33] E.T. Grygielko, W.M. Martin, C. Tweed, P. Thornton, J. Harling, D.P. Brooks, N. J. Laping, Inhibition of gene markers of fibrosis with a novel inhibitor of transforming growth factor-beta type I receptor kinase in puromycin-induced nephritis, J. Pharmacol. Exp. Ther. 313 (2005) 943–951, https://doi.org/10.1124/jpet.104.082099.
[34] Z.G. Fridlender, J. Sun, S. Kim, V. Kapoor, G. Cheng, L. Ling, G.S. Worthen, S. M. Albelda, Polarization of tumor-associated neutrophil phenotype by TGF-beta: "N1" versus "N2" TAN, Cancer Cell 16 (2009) 183–194, https://doi.org/10.1016/j.ccr.2009.06.017.
[35] S.K. Wculek, I. Malanchi, Neutrophils support lung colonization of metastasis-initiating breast cancer cells, Nature 528 (2015) 413–417, https://doi.org/10.1038/nature16140.
[36] K. Donati, C. Sepult, N. Rocks, S. Blacher, C. Gerard, A. Noel, D. Cataldo, Neutrophil-derived interleukin 16 in premetastatic lungs promotes breast tumor cell seeding, Cancer Growth Metastasis 10 (2017), 1179064417738513, https://doi.org/10.1177/1179064417738513.
[37] J. Jablonska, S. Lang, R.V. Sionov, Z. Granot, The regulation of pre-metastatic niche formation by neutrophils, Oncotarget 8 (2017) 112132–112144, https://doi.org/10.18632/oncotarget.22792.
[38] H.H. Yan, M. Pickup, Y. Pang, A.E. Gorska, Z. Li, A. Chytil, Y. Geng, J.W. Gray, H. L. Moses, L. Yang, Gr-1+CD11b+ myeloid cells tip the balance of immune protection to tumor promotion in the premetastatic lung, Cancer Res. 70 (2010) 6139–6149, https://doi.org/10.1158/0008-5472.CAN-10-0706.
[39] J.Y. Sagiv, J. Michaeli, S. Assi, I. Mishalian, H. Kisos, L. Levy, P. Damti, D. Lumbroso, L. Polyansky, R.V. Sionov, A. Ariel, A.H. Hovav, E. Henke, Z. G. Fridlender, Z. Granot, Phenotypic diversity and plasticity in circulating neutrophil subpopulations in cancer, Cell Rep. 10 (2015) 562–573, https://doi.org/10.1016/j.celrep.2014.12.039.
[40] N. Borregaard, L. Kjeldsen, H. Sengelov, M.S. Diamond, T.A. Springer, H. C. Anderson, T.K. Kishimoto, D.F. Bainton, Changes in subcellular-localization and surface expression of L-selectin, alkaline-phosphatase, and mac-1 in human neutrophils during stimulation with inflammatory mediators, J. Leukoc. Biol. 56 (1994) 80–87, https://doi.org/10.1002/jlb.56.1.80.
[41] M.E. Shaul, L. Levy, J. Sun, I. Mishalian, S. Singhal, V. Kapoor, W. Horng, G. Fridlender, S.M. Albelda, Z.G. Fridlender, Tumor-associated neutrophils display a distinct N1 profile following TGFbeta modulation: a transcriptomics analysis of pro- vs. antitumor TANs, Oncoimmunology 5 (2016), e1232221, https://doi.org/10.1080/2162402X.2016.1232221.
[42] J. Park, R.W. Wysocki, Z. Amoozgar, L. Maiorino, M.R. Fein, J. Jorns, A.F. Schott, Y. Kinugasa-Katayama, Y. Lee, N.H. Won, E.S. Nakasone, S.A. Hearn, V. Kuttner, J. Qiu, A.S. Almeida, N. Perurena, K. Kessenbrock, M.S. Goldberg, M. Egeblad, Cancer cells induce metastasis-supporting neutrophil extracellular DNA traps, Sci. Transl. Med. 8 (2016) 361, ra138, https://doi.org/10.1126/scitranslmed.aag1711.
[43] M.E. Shaul, Z.G. Fridlender, Tumour-associated neutrophils in patients with cancer, Nat. Rev. Clin. Oncol. 16 (2019) 601–620, https://doi.org/10.1038/s41571-019-0222-4.
[44] V. Papayannopoulos, Neutrophil extracellular traps in immunity and disease, Nat. Rev. Immunol. 18 (2018) 134–147, https://doi.org/10.1038/nri.2017.105.
[45] B. De Craene, G. Berx, Regulatory networks defining EMT during cancer initiation and progression, Nat. Rev. Cancer 13 (2013) 97–110, https://doi.org/10.1038/nrc3447.
[46] A. Puisieux, T. Brabletz, J. Caramel, Oncogenic roles of EMT-inducing transcription factors, Nat. Cell Biol. 16 (2014) 488–494, https://doi.org/10.1038/ncb2976.
[47] A. Moustakas, C.H. Heldin, Mechanisms of TGFbeta-induced epithelial-mesenchymal transition, J. Clin. Med. 5 (2016), https://doi.org/10.3390/jcm5070063.
[48] M. Wu, H. Zhang, C. Tie, C. Yan, Z. Deng, Q. Wan, X. Liu, F. Yan, H. Zheng, MR imaging tracking of inflammation-activatable engineered neutrophils for targeted therapy of surgically treated glioma, Nat. Commun. 9 (2018) 4777, https://doi.org/10.1038/s41467-018-07250-6.
[49] S.H. Wrzesinski, Y.S.Y. Wan, R.A. Flavell, Transforming growth factor-beta and the immune response: implications for anticancer therapy, Clin. Cancer Res. 13 (2007) 5262–5270, https://doi.org/10.1158/1078-0432.CCR-07-1157.
[50] R.B. Holmgaard, D.A. Schaer, Y. Li, S.P. Castaneda, M.Y. Murphy, X. Xu, I. Inigo, J. Dobkin, J.R. Manro, P.W. Iversen, D. Surguladze, G.E. Hall, R.D. Novosiadly, K. A. Benhadji, G.D. Plowman, M. Kalos, K.E. Driscoll, Targeting the TGFbeta pathway with galunisertib, a TGFbetaRI small molecule inhibitor, promotes anti-tumor immunity leading to durable, complete responses, as monotherapy and in combination with checkpoint blockade, J. Immunother. Cancer 6 (2018) 47, https://doi.org/10.1186/s40425-018-0356-4.
[51] K.A. West, C. Conry-Cantilena, Granulocyte transfusions: current science and perspectives, Semin. Hematol. 56 (2019) 241–247, https://doi.org/10.1053/j.seminhematol.2019.11.002.
[52] C. Konstantakis, P. Tselekouni, M. Kalafateli, C. Triantos, Vitamin D deficiency in patients with liver cirrhosis, Ann. Gastroenterol. 29 (2016) 297–306, https://doi.org/10.20524/aog.2016.0037.
[53] D. Maharaj, P.G. Vianna, W. Ward, A.J. Messina, T. Rayborn, J.V. Gouvea, R. D. Hammer, Z. Cui, Young donor white blood cell immunotherapy induces extensive tumor necrosis in advanced-stage solid tumors, Heliyon 3 (2017), e00438, https://doi.org/10.1016/j.heliyon.2017.e00438.